Polymer Testing 114 (2022) 107687

Contents lists available at ScienceDirect

Polymer Testing

journal homepage: www.elsevier.com/locate/polytest

Piezoresistive sensing performance of multifunctional MWCNT/HDPE auxetic structures enabled by additive manufacturing

Sara AlMahri [a], Johannes Schneider [b], Andreas Schiffer [c], S. Kumar [b,*]

[a] Advanced Material Research Center, Technology Innovation Institute, Masdar City, P.O. Box 9639, Abu Dhabi, United Arab Emirates
[b] James Watt School of Engineering, University of Glasgow, Glasgow G12 8QQ, UK
[c] Department of Mechanical Engineering, Khalifa University of Science and Technology, Abu Dhabi, 127788, United Arab Emirates

ARTICLE INFO

Keywords:
3D printing
Multi-functional composite
Strain- and damage-sensing
Self-sensing
Nanocomposite

ABSTRACT

Herein, we report the mechanical and piezoresistive sensing performance of 3D printed auxetic nanocomposite structures composed of a high-density polyethylene (HDPE) matrix and multi-walled carbon nanotubes (MWCNTs). The multifunctional performance of MWCNT/HDPE auxetic structures were measured under tensile loading. The results indicate that by varying the MWCNT content, as well as the relative density and cell topology (S-shaped, Chiral and Re-entrant) of the structure, we can achieve a tunable piezoresistive response. The results indicate that the S-shaped cellular structure possesses superior mechanical and piezoresistive characteristics, reporting a gauge factor of 7.6 at 4 wt % MWCNT loading, which is ~300% higher than those measured for the Re-entrant and Chiral structures. We also present an empirical scaling equation that relates the structure's sensitivity factor to its relative density. The findings of this study provide useful guidelines for the design and fabrication of self-sensing smart materials and structures with tunable sensitivity.

1. Introduction

Soft and flexible piezoresistive strain sensors have recently attracted considerable research interest due to their ability to convert mechanical stimuli to readable electric signals in applications such as soft robotics, healthcare monitoring and wearable devices [1–3]. Recently, many electrically-conductive polymer nanocomposites have been explored for high-performance flexible piezoresistive sensors owing to their low cost, good flexibility and excellent mechanical properties [4]. Among various conductive nanofillers, carbon nanotubes (CNTs) possess excellent electrical, thermal and mechanical properties [5,6], which can be exploited to enhance the mechanical, thermal and electrical properties of polymers. Apart from strain sensing, electrically-conductive polymer nanocomposites have also been used in other applications, including damage sensing, interference shielding [7,8] and flexible electronics [9].

One of the most critical design parameters for the piezoresistive sensors is the material's sensitivity to strain, a property referred to in the literature as the gauge factor (GF). In nanocomposites, the GF is controlled by morphological changes in the conductive network with applied mechanical strain where, for example, increased degree of nanofiller separation is associated with reduced electronic conductivity [10]. Piezoresistivity in CNT-based nanocomposites has been attributed to two key mechanisms: (i) the change in the contact resistance of the percolating network induced by the loss of contact between CNTs [11,12], and (ii) changes in the tunnelling resistance which occurs due to distance changes between adjacent CNTs [12–14]. The contact resistance between CNTs, is attributed to the contacting interfaces, as opposed to the intrinsic resistance, or tunneling resistance. While these mechanisms are well understood, it still remains a challenge to achieve high sensitivity factors over a wide range of strains [15]. Recent approaches to improve sensing performance include the incorporation of thermo-expandable microspheres into polymer/CNT composites [16], alignment of nickel particles in rubber/CNT composites [17] and incorporation of silicon dioxide micro-particles [18]. Typically, under applied tensile strain, the conductive nanofillers tend to separate in the direction of applied strain, while the lateral contraction (due to the Poisson's effect) brings the nanofillers closer together, giving rise to two competing effects influencing the piezoresistive sensitivity of the nanocomposite. To further enhance the sensitivity of stretchable strain sensors, recent works have investigated the performance of auxetic structures for strain sensing applications [19–22].

Auxetic structures are lattice structures composed of carefully designed 2D or 3D unit cells [23,24]. They exhibit a negative Poisson's

* Corresponding author.
E-mail address: s.kumar@eng.oxon.org (S. Kumar).

https://doi.org/10.1016/j.polymertesting.2022.107687
Received 16 May 2022; Received in revised form 20 June 2022; Accepted 1 July 2022
Available online 5 July 2022

ratio under applied mechanical load. It has been shown that such unique structural response not only enhances certain mechanical properties (e.g. shear modulus [25], indentation resistance [26], fracture resistance [27]) but also contributes to increased piezoresistive sensing performance due to the combined effect of reduced lateral contraction and strain concentration [20]. Since the geometric features of auxetic structures are often complex, their fabrication has long been hampered by the limitations of traditional manufacturing techniques. However, with the emerging additive manufacturing techniques [28–32], complex material architectures can now be realized at relatively low cost, and this has accelerated research efforts on mechanical metamaterials. Although the mechanical characteristics of auxetic structures have been extensively studied in the literature, studies on the piezoresistive sensing performance of 3D printed auxetic nanocomposites are currently lacking.

Herein, we examine the piezoresistive sensing performance of 2D auxetic multi-walled carbon nanotube (MWCNT)/High Density Polyethylene (HDPE) nanocomposites fabricated via fused filament fabrication (FFF) additive manufacturing. Initially, MWCNT/HDPE filaments with various MWCNT loadings (2, 4 and 6 weight percent (wt%)) were fabricated via melt-blending. Using the nanoengineered filaments, MWCNT/HDPE nanocomposite auxetic structures with different relative densities (20, 30 and 40%) and unit cell geometries (Re-entrant, Chiral and S-shaped structure) were fabricated via FFF. The auxetic structures thus obtained were tested under uniaxial tension and their piezoresistive and mechanical properties as a function of their relative density and unit cell geometry were studied. Finally, an empirical scaling equation that relates the piezoresistive sensitivity of the structure to its relative density is presented.

2. Materials and methods

2.1. Preparation of MWCNT/HDPE filament feedstock for additive manufacturing

The MWCNT/HDPE filaments were produced at a diameter of 1.75 mm via melt mixing using a co-rotating Coperion ZSK 18 (Germany) twin-screw extruder. HDPE was provided in pellet form by the Abu Dhabi Polymers Co Ltd (Borouge), UAE, while the MWCNTs were supplied by Applied Nanostructured Solutions LLC, USA. The nanocomposites were prepared by mixing different weight percentages of MWCNT with HDPE to obtain filaments with either 2, 4 or 6 wt% of MWCNT. Further details on the melt-mixing process are given in Section S1 (Supplementary Material), while detailed characterizations of the MWCNT/HDPE filaments can be found in in our recently published work [33]. The dispersion state of MWCNTs in the HDPE matrix affect both mechanical and functional properties of HDPE/CNT composites. To form an electrically conductive network within the HDPE matrix at a lower percolation threshold and to realize optimal mechanical performance, a uniform dispersion of CNTs is required. The dispersion state of CNTs in the HDPE matrix has been analyzed in our previous study via Scanning Electron Microscopy (SEM) [33]. The percolation threshold was calculated as described in our previous study [33] by fitting conductivity data with a power law function using percolation theory [34, 35] as a function of the percent volume of CNTs. A schematic 2D representation of electrically percolated HDPE/CNT nanocomposites with different microstructures representing different dispersion states of CNTs in the matrix is shown in Fig. S2.

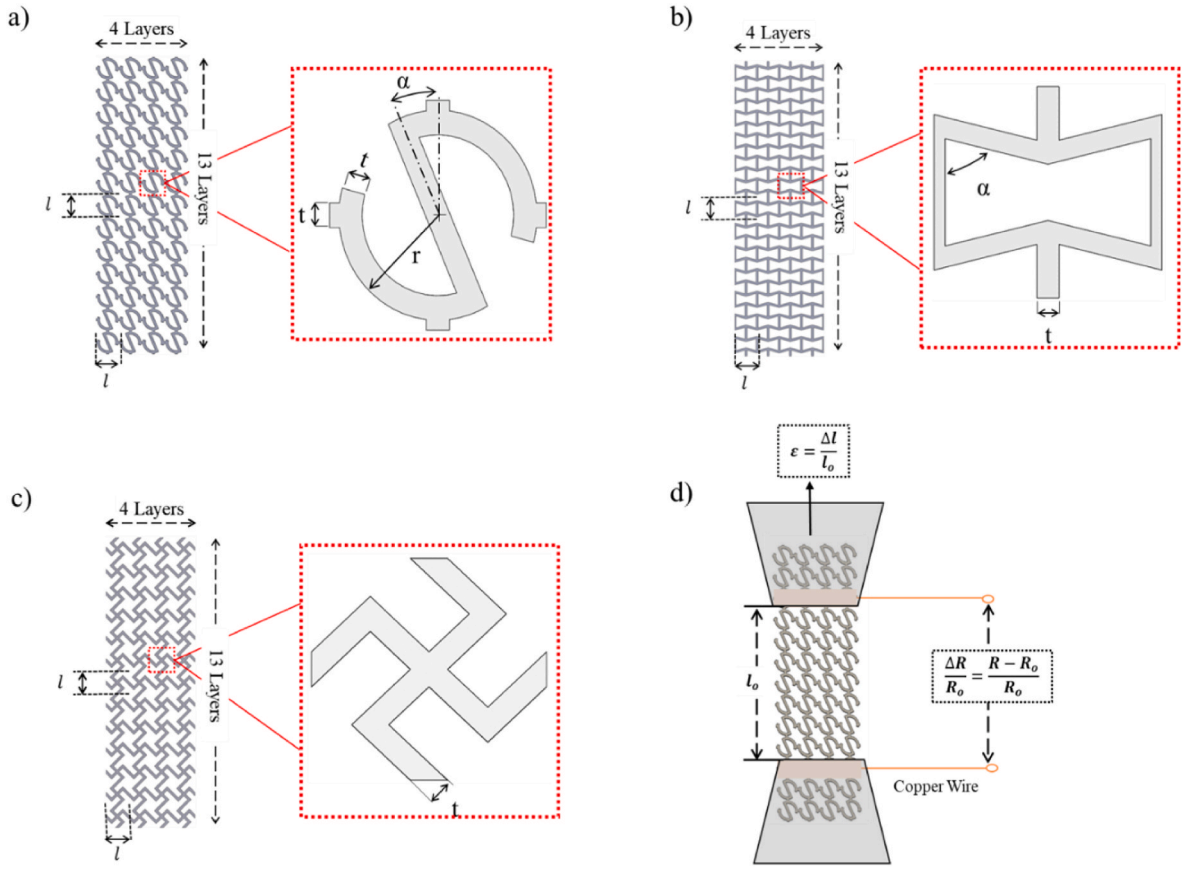

Fig. 1. Auxetic structures with S-shaped (a), Re-entrant (b) and Chiral (c) unit-cell geometry, and a schematic of the piezoresistive test setup (d): ε is the applied strain, l_0 is the initial gauge length over which the change in electrical resistance, $\Delta R = R - R_0$, is measured, where R_0 and R are the resistance at zero strain and at the applied strain, ε, respectively.

2.2. Additive manufacturing of MWCNT/HDPE auxetic structures

The prepared filaments (see Section 2.1) were used to additively manufacture 2D auxetic structures with S-shaped (Fig. 1a), Re-entrant (Fig. 1b) and Chiral (Fig. 1c) unit-cell geometries via FFF. Re-entrant and chiral unit-cell topologies have been widely studied and represent two main mechanisms for achieving auxeticity via unfolding and rotating ligaments, respectively. The recently introduced S-shaped geometry exhibits significantly lower stress concentration under load compared to the re-entrant structure [36]. The designed structures consisted of 4 × 13 unit cells with each unit-cell measuring 7 × 7 × 1 mm, resulting in an overall size of 28 × 91 × 1 mm. For each unit-cell geometry, the in-plane wall thickness, t, was varied to obtain structures of three different relative densities, $\bar{\rho}$ = 20%, 30% or 40%. The major dimensions of each type of structure are listed in Table S1 (Supplementary Material). We used SolidWorks (Dassault Systèmes SolidWorks Corp., USA) to create the CAD models which were then sliced using Simplify3D to prepare them for printing. The auxetic structures were 3D printed via FFF using a Creator Pro 3D printer (Flashforge, USA), depositing the fused filament layer-by-layer on a heated build platform. The auxetic structures were printed using neat HDPE and MWCNT/HDPE composite filaments with 2, 4 and 6 wt% MWCNT loading. For all prints, the nozzle temperature was set to 220 °C, the bed temperature to 120 °C and the layer thickness to 200 μm. In the following, the 3D printed samples are coded as XXYY-Z where XX represents the unit-cell geometry ("S" for S-shaped, "Ch" for chiral and "Re" for re-entrant geometry), YY denotes the relative density in % (either 20, 30 or 40) and Z indicates the MWCNT loading in wt.% (either 2, 4 or 6).

2.3. Mechanical and piezoresistive testing of MWCNT/HDPE auxetic structures

To measure the mechanical and piezoresistive response of the 2D auxetic structures, tensile tests were conducted on the 3D printed samples using a Zwick//Roell Z005 universal testing machine (UTM) with a 2.5 kN load cell. The samples were clamped over an area covering three unit cells at both ends using wedge action grips (see Fig. 1d), resulting in a gauge length of 49 mm, or seven unit cells, while the width is 28 mm, or four unit cells. The representative area for strength and stiffness calculations is calculated by multiplying the width (28 mm) and thickness (1 mm) of the specimen. All experiments were conducted at a strain rate of 0.0017 s^{-1}, allowing for quasi-static tension. Further, we attached two copper sheets to both ends of the sample and connected them to a DMM 4050 multimeter (Tektronix, USA) for *in situ* measurement of sample's electrical resistance, R. Note that the metallic grips of the UTM were insulated from the conductive specimen to ensure that the accuracy of the resistance measurements was not affected by electrical charge leakage. The obtained electrical resistance data were synchronized with the engineering stress and strain measurements, where the strain was deduced from the recorded crosshead displacement. Each test was repeated at least three times to ensure repeatability of the measurements.

3. Results and discussion

3.1. Effect of cell topology on the piezoresistive self-sensing performance

In this section, we examine the effect of the unit-cell geometry on the piezoresistive response of 3D printed MWCNT/HDPE auxetic structures subject to uniaxial tensile loading. We consider auxetic MWCNT/HDPE structures with S-shaped, Chiral and Re-entrant unit-cell geometries (see Fig. 1) and restrict our attention to structures with 40% relative density and 4 wt% MWCNT loading. Note that the mechanical characteristics of these auxetic structures are not discussed here in detail, for the sake of brevity, but are presented in Section S4 (Supplementary Material).

Fig. 2a presents the measured normalized resistance changes, $\Delta R/R_0$, as functions of the applied strain, ε, for the three unit-cell geometries considered here. Here $\Delta R = R - R_0$ denotes the change in the sample's resistance, R, relative to the initial zero-strain resistance, R_0. The figure shows nonlinearities in the piezoresistive responses of the three types of structures characterized by a continuously increasing slope in the measured $\Delta R/R_0$ vs. ε curves, and these nonlinearities become more pronounced at higher strains. As the tensile strain increases, the effective electrical resistance of the auxetic structure increases due to 1) change in contact resistance between CNTs and 2) increase in the distance between the conducting nanofillers, resulting in lower possibilities of forming conductive networks through electron tunnelling (a mechanism which allows electrons to transfer from one CNT to another across a small gap [12]), and this contributes to very high changes in the resistance as the induced strain approaches the failure strain of the material. It can also be seen from Fig. 2a that the S-shaped structures exhibit superior sensitivity to strain when compared to both Chiral and Re-entrant structures. While the Chiral and Re-entrant topologies show a very similar piezoresistive response within the linear elastic regime ($\varepsilon \leq 0.05$), the Chiral structure is slightly more sensitive at higher values of strain. The change in morphology of the conductive network within the cell wall material

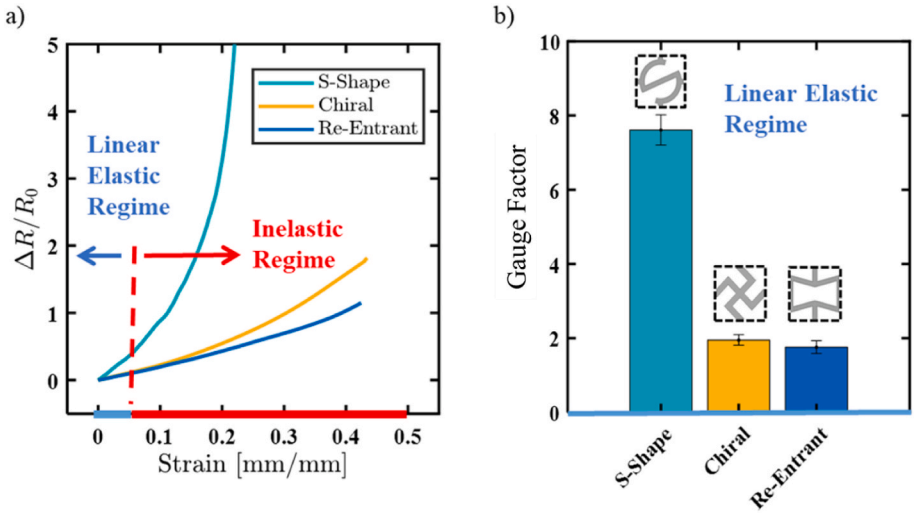

Fig. 2. Effect of cell topology on the piezoresistive response: (a) normalized resistance change plotted as a function of strain, (b) gauge factor evaluated in the linear elastic regime ($\varepsilon < 0.05$).

under tensile load dictates the piezoresistive behavior of all three cellular structures considered herein. The deformation mode of three different unit cell topologies governs their piezoresistive behavior.

To enable a quantitative comparison of the change in electrical resistance to the applied strain, we introduce the gauge factor defined as the slope of the $\Delta R/R_0$ vs. ε curve. Assuming that the piezoresistive response is linear over an interval $[\varepsilon_1, \varepsilon_2]$, the gauge factor can be expressed as

$$k = \frac{(\Delta R_2 - \Delta R_1)/R_0}{\varepsilon_2 - \varepsilon_1} \quad (1)$$

where $\frac{\Delta R_1}{R_0}$ and $\frac{\Delta R_2}{R_0}$ are the resistance changes relative to R_0, evaluated at imposed strains ε_1 and ε_2, respectively. In this study, unless otherwise stated, gauge factors were evaluated within the initial linear elastic regime ($\varepsilon \leq 0.05$).

Based on the data presented in Fig. 2a, the average gauge factors (of at least three repeated tests) corresponding to $\varepsilon \leq 0.05$ are plotted in Fig. 2b for each unit-cell geometry, along with the corresponding error bars (standard deviation). The S-shaped auxetic structure shows an average gauge factor of $k = 7.61$ followed by 1.95 and 1.76 for the Chiral and Re-entrant geometries, respectively, indicating that the S-shaped cellular structure exhibits 300% higher sensitivity to applied strain than the Chiral or Re-entrant structures.

To analyze the piezoresistive sensitivity of the MWCNT/HDPE structures with 4 wt% MWCNT loading over different strain regimes, gauge factors were evaluated from the measurements on five intervals according to eq. (1): [0, 0.05], [0.05, 0.1], [0.1, 0.2], [0.2, 0.3] and [0.3, 0.4]. The obtained values are listed in Table S4 (Supplementary Material), showing that the gauge factors increase steadily with increasing strain for both the S-shaped and Chiral structures, as also seen from Fig. 2a. The gauge factors of the Re-entrant structure, however, remain nearly constant up to large strain (i.e. $\varepsilon = 0.4$), indicating a linear piezoresistive response. While the piezoresistivity of the printed structures within the linear elastic regime (i.e. $\varepsilon \leq 0.05$) can be exploited for strain sensing, the observed resistance changes beyond the yield point ($\varepsilon > 0.05$) are related to irreversible deformation processes, and can be used for damage sensing (Table 1). It is interesting to note that the gauge factor varies with the cell topology (Fig. 2b) in a very similar way as the elastic modulus (Fig. S5b, Supplementary Material), indicating a direct relation between elastic stiffness and piezoresistive sensitivity. The reason for the superior elastic stiffness and strain sensitivity of the S-shaped structure can be explained as follows. As seen from Fig. 1a, the struts of the S-shaped structure that lie within the tensile load path are nearly vertical and therefore, carry the load more efficiently as compared to the Re-entrant or Chiral structure where the load-carrying ligaments are more angled, resulting in a pronounced bend-dominated behavior associated with reduced stiffness. Hence, the struts of the S-shaped structure experience less bending and shearing, and this, in turn, yields enhanced sensing performance since the percolating network of nanofillers is subject to a more uniform stretch-dominated mode of deformation.

Table 1
Mechanical and piezoresistive properties of S-shaped MWCNT/HDPE structures.

Parameter	4 wt%			6 wt%		
Relative density [%]	20	30	40	20	30	40
Young's Modulus [MPa]	23.08 ± 6.0	35.60 ± 5.7	113.25 ± 5.3	22.7 ± 1.9	34.80 ± 2.0	108.35 ± 5.30
Strength [MPa]	1.93 ± 0.70	1.94 ± 0.70	4.89 ± 0.20	0.69 ± 0.04	1.22 ± 0.09	2.13 ± 0.42
Gauge Factor	4.07 ± 1.50	6.40 ± 1.80	7.61 ± 0.41	2.15 ± 0.42	4.22 ± 1.50	5.61 ± 0.17

3.2. Effect of MWCNT loading on the piezoresistive self-sensing performance

We proceed to examine the effect of MWCNT loading on the piezoresistive characteristics of 3D printed MWCNT/HDPE auxetic structures. In Fig. 3a, we plot the no-load resistance, R_0, of S-shaped MWCNT/HDPE structures with different MWCNT loadings (2, 4 or 6%) and constant relative density (40%). As the MWCNT loading increases, the no-load resistance decreases significantly, reporting $R_0 = 60$ kΩ at 2 wt% (which is near the percolation concentration of these 3D printed nanocomposites, see Ref. [33]), $R_0 = 5$ kΩ at 4 wt% and $R_0 = 1.5$ kΩ at 6 wt%. This is expected because a higher MWCNT concentration in the composite results in the formation of additional contact and tunnelling junctions between the conductive MWCNT nanofillers and facilitates the formation of a stable conductive network in the otherwise electrically non-conducting HDPE matrix.

Fig. 3b presents the measured normalized electrical resistance changes, $\Delta R/R_0$, as functions of the applied strain, ε, for S-shaped, Chiral and Re-entrant structures with two different MWCNT loadings (4 wt% and 6 wt%) and constant relative density (40%). Note that the strain range is limited to the linear elastic regime (i.e. $\varepsilon < 0.05$) where strain sensing is appropriate. We also note that $\Delta R/R_0$ values for structures with 2 wt% MWCNT loading (i.e. just above the percolation threshold) are not reported here and in the following figures due to the fact that the electrical resistance of a nanocomposite close to the percolation threshold is highly sensitive to the applied strain, and such high sensitivity could not be accurately captured with our instrument due to its limitation. It is seen from Fig. 3b that the MWCNT/HDPE structures with 4 wt% of MWCNT show higher changes in resistance as compared to those with 6 wt%, and this trend is consistent for all unit cell geometries considered here. The observed increase of the sensitivity with decreasing MWCNT concentration is in line with previous studies (see e.g. Refs. [9,37–40]) and can be explained by the fact that, at lower nanofiller concentrations, the number of conducting channels in the percolating network is smaller and the distances between the nanofillers in each channel also increases (on average), which, in turn, increases the probability of breaking the electron transfer in a channel when tensile strain is applied.

3.3. Effect of relative density on the piezoresistive self-sensing performance

In this section, we explore effects of relative density on the mechanical and piezoresistive characteristics of MWCNT/HDPE S-shaped structures. Note that the influence of relative density on the piezoresistive performance of Chiral and Re-entrant structures is presented in the Supplementary Material (see Section S6).

In Fig. 4a and c we present the stress vs. strain responses of MWCNT/HDPE S-shaped structures with 4 and 6 wt% MWCNT loading, respectively; contours are included for three different relative densities, 20% (blue), 30% (red) and 40% (yellow), respectively. It can be seen that both the Young's modulus and ultimate strength of the auxetic structures increase with increasing relative density (see, Fig. 4e and f), as expected [41]. We also observe a decrease in the failure strain with increasing relative density (see Fig. 4a), except for the composite with 6 wt% MWCNT loading where the sample with 30% relative density shows the largest strain at failure (see Fig. 4c). This inconsistency is believed to have resulted from stochastic nature of defect-structure (i.e., inter- and intra-bead porosities) associated with additive manufacturing. Note that the defect-structure becomes pronounced with increase in MWCNT loading. The structures with 4 wt% MWCNT loading show higher failure strains and more pronounced nonlinearities in their stress vs. strain responses (Fig. 4a) as compared to the ones with 6 wt% MWCNT loading (Fig. 4d), indicating that plastic deformation in the

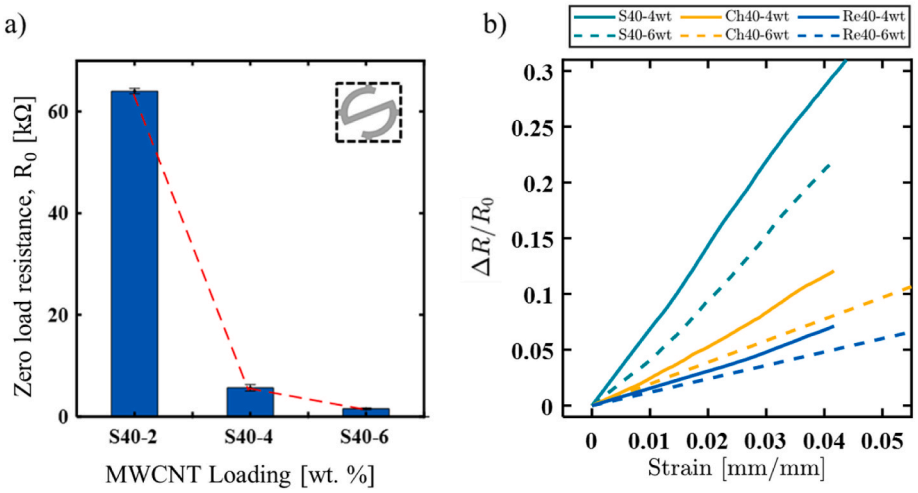

Fig. 3. (a) Initial no-load resistance values, R_0, obtained for S-shaped samples comprising 2, 4 and 6 wt% of MWCNT with a relative density of 40% and (b) normalized resistance change plotted as a function of strain for S-shaped, Chiral and Re-entrant samples comprising 4 and 6 wt% MWCNT with a relative density of 40%; the strain rage is restricted to the linear elastic regime ($\varepsilon < 5\%$).

composite was highly restricted when the MWCNT loading reached 6 wt % MWCNT, and this is corroborated by the stress vs. strain responses obtained from dogbone specimens (see Fig. S4, Supplementary Material). In Fig. 4e–f, we show, respectively, the average Young's modulus and ultimate strength values extracted from three repeated tests. Comparing the modulus and strength data of the structures with 4 wt% and 6 wt% MWCNT loading, we detect only minor differences in the Young's modulus (Fig. 4e) but large discrepancies in the ultimate strength (Fig. 4f). This can be explained by the lower ductility of the composite with 6 wt% MWCNT loading (Fig. S4, Supplementary Material) which makes the material more prone to brittle fracture around existing defects that act as stress raisers. We also notice a slight decrease in the Young's modulus with an increase in the MWCNT loading from 4 to 6 wt%; this can be attributed to the lower printing quality of 6 wt% MWCNT/HDPE structures which resulted in a larger number of defects in the FDM print (see Fig. S8, Supplementary Material). Table 1 summarizes the mechanical properties (tensile strength and Young's modulus measurements plotted in Fig. 4e–f) of the auxetic structures under tensile loading. Note that the measured Young's moduli E were found to be well described by the Gibson-Ashby [41] model

$$\frac{E}{E_s} = C\left(\frac{\rho}{\rho_s}\right)^n \tag{2}$$

where E_s and ρ_s are the modulus and density of the parent material respectively, E and ρ are the modulus and density of the cellular structure respectively, ρ/ρ_s represents the relative density, and C and n are constants that are typically found via curve fitting. Least-square fits of eq. (2) to our measurements (see Fig. S7, Supplementary Material) yielded $n = 2.21$ and $n = 2.18$ for S-shaped structures with 4 and 6 wt% MWCNT loading, respectively, which lie within the expected range of bend-dominated lattices [41].

Fig. 4b and d presents the piezoresistance measurements of S-shaped MWCNT/HDPE structures with 4 and 6 wt% MWCNT loading respectively for three different relative densities. These figures show that $\Delta R/R_0$ becomes more sensitive to variations in strain with increasing relative density; for the S-shaped structure with 4 wt % MWCNT loading, we report a 87% increase in gauge factor (from 4.07 to 7.61) with an increase in the relative density from 20 to 40% (see Fig. 4g). It is worth noting that the $\Delta R/R_0$ vs. ε responses of S-shaped structures with 6 wt% MWCNT loading (Fig. 4d) do not show the nonlinearities that we observe for those with 4 wt% MWCNT loading. This can be explained by the limited ductility of the MWCNT/HDPE composite with 6 wt% MWCNT loading, which resulted in sudden failure of the structure under a small, imposed strain ($\varepsilon < 0.1$) where the connectivity of the percolating network is maintained, and changes in the tunnelling resistance remain small.

The observed increase in the gauge factor with increasing relative density (see Fig. 4g) can be attributed to the higher number of conducting paths available in higher relative density structures. In fact, an increase in relative density can be imagined as the inclusion of additional conducting paths in parallel, all of which undergoing the same strain under tensile loading. As a result, a lattice structure with higher relative density possesses a lower no-load resistance, R_0, as compared to the one with lower relative density, as seen from Table 1 and Fig. 5b. Assuming a uniform dispersion of nanofillers, it is expected that all conductive paths in the percolating network of a lattice structure would become non-conducting at nearly the same level of applied strain, irrespective of the relative density chosen. Consequently, $\Delta R/R_0$ in a lattice structure with higher relative density is expected to be larger over an increment of strain since 1) its no-load resistance is lower than that of a lower relative density structure and 2) breakage of large number of conductive paths in the high relative density structure compared to those in lower relative density structures of same MWCNT content. Therefore, we could expect increase in the gauge factor with increasing relative density, as observed from our measurements. The synchronized mechanical and piezoresistive response with deformation maps of S-shaped and Chiral cellular structures (4 wt% MWCNT loading) can be seen in the Video SV1.

To further investigate the coupling between piezoresistive performance and the relative density of a lattice structure, we plot, in Fig. 5a, the gauge factor as a function of relative density for S-shaped, Chiral and Re-entrant lattice structures with 4 wt% and 6 wt% MWCNT loading. By performing least-square fits to the measured data, we find that the effect of relative density on the gauge factor can be described by a power-law relation

$$\frac{k}{k_s} = a\left(\frac{\rho}{\rho_s}\right)^b \tag{3}$$

where k/k_s is the normalized gauge factor with k_s being the gauge factor of the parent material, ρ/ρ_s is the relative density, and a and b are fitting parameters with their numerical values listed in Table S5 (Supplementary Material). While eq. (3) provides a good description of the data plotted in Fig. 5a, it is noted that k/k_s does not approach unity when $\rho/\rho_s \to 1$, as we would expect; hence, the simple power-law relation in eq. (3) would not be suitable for lattice structures with high relative density (i.e. $> 50\%$).

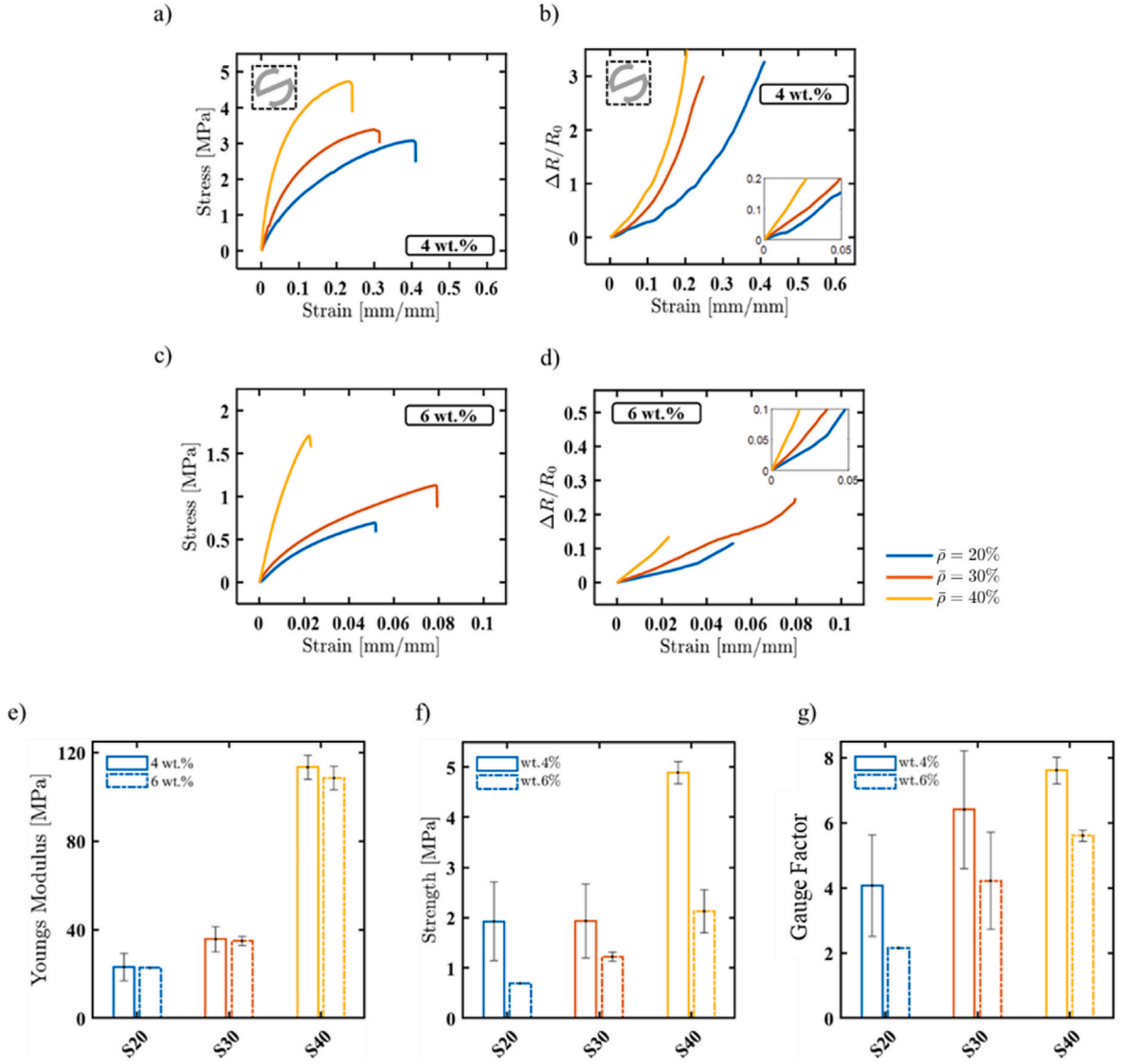

Fig. 4. Stress vs. strain responses of S-shaped structures with 4 wt% (a) and 6 wt% (c) MWCNT loading and their corresponding normalized resistance changes as a function of strain (b,d); the bar charts compare the measured Young's modulus (e), ultimate strength (f) and gauge factor (g) between different relative densities and MWCNT loadings of S-shaped structure.

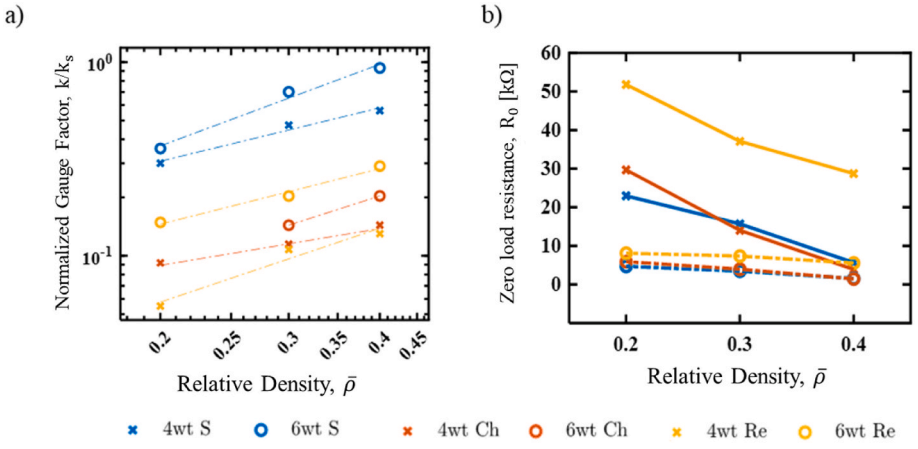

Fig. 5. Normalized gauge factor (a) and initial resistance (b) as functions of relative density for S-shaped, Chiral and Re-entrant nanocomposite structures comprising 4 and 6 wt% MWCNT.

4. Conclusions

In this study, we examined the mechanical characteristics and piezoresistive sensing performance of 3D printed multifunctional auxetic nanocomposite structures composed of a high-density polyethylene (HDPE) matrix reinforced with electrically conductive multi-walled carbon nanotubes (MWCNTs). Auxetic structures with different cell topology and relative densities were additively manufactured via fused filament fabrication (FFF) process using melt-blended MWCNT/HDPE filaments with varying MWCNT weight content. Both mechanical and piezoresistive responses of MWCNT/HDPE auxetic structures were measured under tensile loading. The results showed that the S-shaped cellular structure possesses superior mechanical and piezoresistive characteristics, reporting a gauge factor of 7.6 at 4 wt % MWCNT loading, which is ~300% higher than those measured for the Re-entrant and Chiral structures. It was also shown that the gauge factor of all auxetic structures decreases significantly with increase in MWCNT loading from 4 to 6 wt%. Our results further revealed a strong dependence of the gauge factor upon the relative density of the cellular structure, which was well-described by a simple power-law scaling equation for all cell topologies considered herein. The findings of this study provide useful guidelines for the design and fabrication of self-sensing cellular structures with tunable sensitivity, and this will likely stimulate further research into 3D printed micro-architected smart materials for a broad range of applications, including wearable electronics and self-sensing prosthetics.

Data availability

The raw/processed data required to reproduce these findings cannot be shared at this time due to technical or time limitations.

CRediT authorship contribution statement

Sara AlMahri: Data curation, Writing – original draft. **Johannes Schneider:** Data curation, Writing – original draft, Writing – review & editing. **Andreas Schiffer:** Writing – review & editing. **S. Kumar:** Conceptualization, Methodology, Writing – review & editing.

Declaration of competing interest

The authors declare that they have no known competing financial interests or personal relationships that could have appeared to influence the work reported in this paper.

Acknowledgments

The authors would like to acknowledge the funding provided by Khalifa University through the Competitive Internal Research Award (CIRA) [grant number: CIRA-2018-128]. This work was supported in part by the UK Engineering and Physical Sciences Research Council (Grant no. EP/R513222/1).

Appendix A. Supplementary data

Supplementary data to this article can be found online at https://doi.org/10.1016/j.polymertesting.2022.107687.

Supplementary Information

Supplementary Information contains details of MWCNT/HDPE filament fabrication via melt-mixing, design of S-shaped, chiral and re-entrant auxetic structures, mechanical and piezoresistive characteristics of 3D printed bulk MWCNT/HDPE nanocomposites, effect of cell topology on the mechanical response of MWCNT/HDPE auxetic structures, scaling relations between elastic modulus and relative density of auxetic structures, piezoresistive characteristics of MWCNT/HDPE auxetic structures with Chiral and Re-entrant cell topologies, gauge factors for different cell topologies over five different strain intervals, fitting parameters for the power-law scaling equation that relates the gauge factor to the relative density, and the Video SV1 that shows the synchronized mechanical and piezoresistive response with deformation maps of S-shaped and Chiral cellular structures (4 wt% MWCNT loading).

References

[1] M. Xie, K. Hisano, M. Zhu, T. Toyoshi, M. Pan, S. Okada, O. Tsutsumi, S. Kawamura, C. Bowen, Flexible multifunctional sensors for wearable and robotic applications, Adv. Mater. Technol. 4 (2019), 1800626, https://doi.org/10.1002/admt.201800626.

[2] Y.A. Samad, Y. Li, A. Schiffer, S.M. Alhassan, K. Liao, Graphene foam developed with a novel two-step technique for low and high strains and pressure-sensing applications, Small 11 (2015) 2380–2385, https://doi.org/10.1002/smll.201403532.

[3] S.P. Patole, S.K. Reddy, A. Schiffer, K. Askar, B.G. Prusty, S. Kumar, Piezoresistive and mechanical characteristics of graphene foam nanocomposites, ACS Appl. Nano Mater. 2 (2019) 1402–1411, https://doi.org/10.1021/acsanm.8b02306.

[4] H. Liu, W. Huang, X. Yang, K. Dai, G. Zheng, C. Liu, C. Shen, X. Yan, J. Guo, Z. Guo, Organic vapor sensing behaviors of conductive thermoplastic polyurethane–graphene nanocomposites, J. Mater. Chem. C 4 (2016) 4459–4469, https://doi.org/10.1039/C6TC00987E.

[5] M.F. Arif, S. Kumar, T. Shah, Tunable morphology and its influence on electrical, thermal and mechanical properties of carbon nanostructure-buckypaper, Mater. Des. 101 (2016) 236–244, https://doi.org/10.1016/j.matdes.2016.03.122.

[6] J.M. Wernik, S.A. Meguid, Recent developments in multifunctional nanocomposites using carbon nanotubes, Appl. Mech. Rev. 63 (2011), https://doi.org/10.1115/1.4003503.

[7] P. Verma, T. Bansala, S.S. Chauhan, D. Kumar, S. Deveci, S. Kumar, Electromagnetic interference shielding performance of carbon nanostructure reinforced, 3D printed polymer composites, J. Mater. Sci. 56 (2021) 11769–11788, https://doi.org/10.1007/s10853-021-05985-0.

[8] P. Verma, P. Saini, R.S. Malik, V. Choudhary, Excellent electromagnetic interference shielding and mechanical properties of high loading carbon-nanotubes/polymer composites designed using melt recirculation equipped twin-screw extruder, Carbon N. Y. 89 (2015) 308–317, https://doi.org/10.1016/j.carbon.2015.03.063.

[9] S. Kumar, T.K. Gupta, K.M. Varadarajan, Strong, stretchable and ultrasensitive MWCNT/TPU nanocomposites for piezoresistive strain sensing, Compos. B Eng. 177 (2019), 107285, https://doi.org/10.1016/J.COMPOSITESB.2019.107285.

[10] S. Béfahy, S. Yunus, T. Pardoen, P. Bertrand, M. Troosters, Stretchable helical gold conductor on silicone rubber microwire, Appl. Phys. Lett. 91 (2007), 141911, https://doi.org/10.1063/1.2793185.

[11] T.K. Gupta, M. Choosri, K.M. Varadarajan, S. Kumar, Self-sensing and mechanical performance of CNT/GNP/UHMWPE biocompatible nanocomposites, J. Mater. Sci. 53 (2018) 7939–7952, https://doi.org/10.1007/s10853-018-2072-3.

[12] M. Park, H. Kim, J.P. Youngblood, Strain-dependent electrical resistance of multi-walled carbon nanotube/polymer composite films, Nanotechnology 19 (2008), 055705, https://doi.org/10.1088/0957-4484/19/05/055705.

[13] T.K. Gupta, S. Kumar, A.Z. Khan, K.M. Varadarajan, W.J. Cantwell, Self-sensing performance of MWCNT-low density polyethylene nanocomposites, Mater. Res. Express 5 (2018), 15703.

[14] B. De Vivo, P. Lamberti, G. Spinelli, V. Tucci, L. Vertuccio, V. Vittoria, Simulation and experimental characterization of polymer/carbon nanotubes composites for strain sensor applications, J. Appl. Phys. 116 (2014), 054307, https://doi.org/10.1063/1.4892098.

[15] A. Larmagnac, S. Eggenberger, H. Janossy, J. Vörös, Stretchable electronics based on Ag-PDMS composites, Sci. Rep. 4 (2015) 7254, https://doi.org/10.1038/srep07254.

[16] J.-H. Cai, J. Li, X.-D. Chen, M. Wang, Multifunctional polydimethylsiloxane foam with multi-walled carbon nanotube and thermo-expandable microsphere for temperature sensing, microwave shielding and piezoresistive sensor, Chem. Eng. J. 393 (2020), 124805, https://doi.org/10.1016/j.cej.2020.124805.

[17] Y.-F. Chen, M.-L. Huang, J.-H. Cai, Y.-X. Weng, M. Wang, Piezoresistive anisotropy in conductive silicon rubber/multi-walled carbon nanotube/nickel particle composites via alignment of nickel particles, Compos. Sci. Technol. 225 (2022), 109520, https://doi.org/10.1016/j.compscitech.2022.109520.

[18] Y.-F. Chen, J. Li, Y.-J. Tan, J.-H. Cai, X.-H. Tang, J.-H. Liu, M. Wang, Achieving highly electrical conductivity and piezoresistive sensitivity in polydimethylsiloxane/multi-walled carbon nanotube composites via the incorporation of silicon dioxide micro-particles, Compos. Sci. Technol. 177 (2019) 41–48, https://doi.org/10.1016/j.compscitech.2019.04.017.

[19] H.W. Kim, T.Y. Kim, H.K. Park, I. You, J. Kwak, J.C. Kim, H. Hwang, H.S. Kim, U. Jeong, Hygroscopic auxetic on-skin sensors for easy-to-handle repeated daily use, ACS Appl. Mater. Interfaces 10 (2018) 40141–40148, https://doi.org/10.1021/acsami.8b13857.

[20] Y. Jiang, Z. Liu, N. Matsuhisa, D. Qi, W.R. Leow, H. Yang, J. Yu, G. Chen, Y. Liu, C. Wan, Z. Liu, X. Chen, Auxetic mechanical metamaterials to enhance sensitivity

of stretchable strain sensors, Adv. Mater. 30 (2018), 1706589, https://doi.org/10.1002/adma.201706589.
[21] M.F. Ahmed, Y. Li, C. Zeng, Stretchable and compressible piezoresistive sensors from auxetic foam and silver nanowire, Mater. Chem. Phys. 229 (2019) 167–173, https://doi.org/10.1016/j.matchemphys.2019.03.015.
[22] B. Taherkhani, M.B. Azizkhani, J. Kadkhodapour, A.P. Anaraki, S. Rastgordani, Highly sensitive, piezoresistive, silicone/carbon fiber-based auxetic sensor for low strain values, Sensors Actuators A Phys 305 (2020), 111939, https://doi.org/10.1016/j.sna.2020.111939.
[23] J.N. Grima, A. Alderson, K.E. Evans, An alternative explanation for the negative Poisson's ratios in auxetic foams, J. Phys. Soc. Japan. 74 (2005) 1341–1342, https://doi.org/10.1143/JPSJ.74.1341.
[24] C. Smith, J. Grima, K. Evans, A novel mechanism for generating auxetic behaviour in reticulated foams: missing rib foam model, Acta Mater. 48 (2000) 4349–4356, https://doi.org/10.1016/S1359-6454(00)00269-X.
[25] K.E. Evans, A. Alderson, Auxetic materials: functional materials and structures from lateral thinking, Adv. Mater. 12 (2000) 617–628, https://doi.org/10.1002/(SICI)1521-4095(200005)12:9<617::AID-ADMA617>3.0.CO;2-3.
[26] K.L. Alderson, A. Fitzgerald, K.E. Evans, The strain dependent indentation resilience of auxetic microporous polyethylene, J. Mater. Sci. 35 (2000) 4039–4047, https://doi.org/10.1023/A:1004830103411.
[27] J.N. Grima, K.E. Evans, Auxetic behavior from rotating squares, J. Mater. Sci. Lett. 19 (2000) 1563–1565, https://doi.org/10.1023/A:1006781224002.
[28] P. Verma, J. Ubaid, K.M. Varadarajan, B.L. Wardle, S. Kumar, Synthesis and characterization of carbon nanotube-doped thermoplastic nanocomposites for the additive manufacturing of self-sensing piezoresistive materials, ACS Appl. Mater. Interfaces 14 (2022) 8361–8372, https://doi.org/10.1021/acsami.1c20491.
[29] J.J. Andrew, H. Alhashmi, A. Schiffer, S. Kumar, V.S. Deshpande, J. Jefferson Andrew, H. Alhashmi, A. Schiffer, S. Kumar, V.S. Deshpande, J.J. Andrew, H. Alhashmi, A. Schiffer, S. Kumar, V.S. Deshpande, Energy absorption and self-sensing performance of 3D printed CF/PEEK cellular composites, Mater. Des. 208 (2021), 109863, https://doi.org/10.1016/j.matdes.2021.109863.
[30] P. Verma, A. Schiffer, S. Kumar, Thermo-resistive and thermo-piezoresistive sensitivity of carbon nanostructure engineered thermoplastic composites processed via additive manufacturing, Polym. Test. 93 (2021), 106961, https://doi.org/10.1016/j.polymertesting.2020.106961.
[31] S. AlMahri, R. Santiago, D.-W. Lee, H. Ramos, H. Alabdouli, M. Alteneiji, Z. Guan, W. Cantwell, M. Alves, Evaluation of the dynamic response of triply periodic minimal surfaces subjected to high strain-rate compression, Addit. Manuf. 46 (2021), 102220, https://doi.org/10.1016/j.addma.2021.102220.
[32] J. Ubaid, J. Schneider, V.S. Deshpande, B.L. Wardle, S. Kumar, Multifunctionality of nanoengineered self-sensing lattices enabled by additive manufacturing, Adv. Eng. Mater. n/a (2022), 2200194, https://doi.org/10.1002/adem.202200194.
[33] A. Mora, P. Verma, S. Kumar, Electrical conductivity of CNT/polymer composites: 3D printing, measurements and modeling, Compos. B Eng. 183 (2020), 107600, https://doi.org/10.1016/J.COMPOSITESB.2019.107600.
[34] F. Alam, M. Choosri, T.K. Gupta, K.M. Varadarajan, D. Choi, S. Kumar, Electrical, mechanical and thermal properties of graphene nanoplatelets reinforced UHMWPE nanocomposites, Mater. Sci. Eng. B 241 (2019) 82–91, https://doi.org/10.1016/j.mseb.2019.02.011.
[35] E.T. Thostenson, C. Li, T.-W. Chou, Nanocomposites in context, Compos. Sci. Technol. 65 (2005) 491–516, https://doi.org/10.1016/j.compscitech.2004.11.003.
[36] K. Meena, S. Singamneni, A new auxetic structure with significantly reduced stress concentration effects, Mater. Des. 173 (2019), 107779, https://doi.org/10.1016/j.matdes.2019.107779.
[37] M.F. Arif, S. Kumar, T.K. Gupta, K.M. Varadarajan, Strong linear-piezoresistive-response of carbon nanostructures reinforced hyperelastic polymer nanocomposites, Compos. Part A Appl. Sci. Manuf. 113 (2018) 141–149, https://doi.org/10.1016/J.COMPOSITESA.2018.07.021.
[38] S.K. Reddy, S. Kumar, K.M. Varadarajan, P.R. Marpu, T.K. Gupta, M. Choosri, Strain and damage-sensing performance of biocompatible smart CNT/UHMWPE nanocomposites, Mater. Sci. Eng. C 92 (2018) 957–968, https://doi.org/10.1016/j.msec.2018.07.029.
[39] J.R. Bautista-Quijano, P. Pötschke, H. Brünig, G. Heinrich, Strain sensing, electrical and mechanical properties of polycarbonate/multiwall carbon nanotube monofilament fibers fabricated by melt spinning, Polymer (Guildf) 82 (2016) 181–189, https://doi.org/10.1016/j.polymer.2015.11.030.
[40] M. Haghgoo, M.K. Hassanzadeh-Aghdam, R. Ansari, A comprehensive evaluation of piezoresistive response and percolation behavior of multiscale polymer-based nanocomposites, Compos. Part A Appl. Sci. Manuf. 130 (2020), 105735, https://doi.org/10.1016/j.compositesa.2019.105735.
[41] L.J. Gibson, M.F. Ashby, Cellular Solids, Cambridge University Press, 1997, https://doi.org/10.1017/CBO9781139878326.